Final Draft
of the original manuscript:

Steiner, L.; Bouvier, V.; May, U.; Huber, N.:
Simulation of friction and wear in DLC/steel contacts for different loading histories and geometries: Ball-on-plate configuration and piston–cylinder-contacts
In: Tribology International (2010) Elsevier

DOI: 10.1016/j.triboint.2010.01.012

Simulation of friction and wear in DLC/steel contacts for different loading histories and geometries: ball-on-plate configuration and piston-cylinder-contacts

L. Steiner[a,*], V. Bouvier[a], U. May[a], N. Huber[b,c]

[a] Robert Bosch GmbH, Postfach 106050, 70049 Stuttgart, Germany.

[b] Institut für Werkstoffphysik und Technologie, TUHH, Eißendorfer Str. 42, 21071 Hamburg, Germany.

[c] Institute of Materials Research, GKSS Research Centre Geesthacht, Max-Planck-Str. 1, 21502 Geesthacht, Germany.

Abstract

DLC-coatings are commonly used in industry as a wear protective layer and as a solid lubricant for highly loaded tribological contacts. In order to evaluate the wear performance of different DLC-coatings under unlubricated oscillating sliding wear conditions and to validate the reliability of coated components, many wear-tests with simple model-geometries as well as expensive endurance-tests with the real application conditions have to be performed. This is because the transfer of the wear results to different contact conditions (variation of load, application geometry) is not yet possible. In an earlier paper a novel unified dissipated energy model for the ball-on-plate-geometry was developed and its transferability to different types of coatings was verified. In this paper the model was applied to different load steps and a piston-cylinder-geometry in order to verify its generality. The analytical wear calculation tool - the Global Incremental Wear Model (GIWM) - was revised by considering different load steps and by implementing a new approach for the calculation of wear in the piston-cylinder-contact. Based on the good agreement between the experimental results and both wear and friction simulations, the validity of the unified wear model regarding its transferability to different loading histories and geometries was successfully proven.

Keywords

Wear-modelling, carbon-based coatings, sliding wear, ball-on-plate-contact, piston-cylinder-contact

1. Introduction

During the last twenty years, Diamond-like Carbon- (DLC-) coatings have attracted considerable attention in tribological applications due to their characteristic properties of high wear resistance, high hardness, low friction coefficient, enhanced counterpart protection and chemical inertness. Especially in highly loaded tribological contacts, DLC has the function of a wear protective coating, as it acts as a solid lubricant [1, 2, 3].
A reliable prediction of the coating's lifetime and a determination of the limitations of application represent a great challenge, as they would permit a decrease in the number of endurance tests and consequently lead to cost reductions and faster development.
Since no reliable wear models exist for the calculation of complex DLC-contacts, the coating's performance is currently derived through a sequence of numerous wear tests with different levels of simplification. They range from expensive endurance tests on the real application to simple oscillating ball-on-plate experiments under accelerated conditions (unlubricated, high loads). The simplified experiments allow a rapid classification of the coatings for a specific application, but the transfer of these results to the real application geometry is very difficult.

The derivation of wear models for different materials and contact geometries have been intensively studied in the recent years and numerous, mainly empirical wear models have been developed to calculate the wear [4-12]. However, most of these existing wear models are restricted to the specific contact conditions used for their development. They do not provide the possibility of transferring the model to different geometries or – caused by different processing conditions – to a variation of materials, as it is usually the case in industrial applications. This also applies to the modelling of DLC-contacts [13, 14].

In a previous work [15], we therefore developed an enhanced unified wear model, which was developed and validated with the help of experiments in a ball-on-plate-geometry. It calculates the wear and friction behaviour of DLC-coatings of different roughness, hardness and Young's modulus as well as the wear behaviour of the steel counterpart in an unlubricated oscillating sliding test. We achieved this with an iterative process including modelling, simulations and experiments. The model was validated by means of three different types of DLC-coatings with different degrees of surface roughness.

In this paper, we will prove that our wear model can be transferred to different loading histories and geometries without any further adjustments. It enables lifetime predictions of a component based on accelerated model experiments and allows the designer of a component to evaluate the applicability of a certain coating for a specific application.

The model is based on the dissipated energy approach [11, 12] and the assumption that the dimensional wear coefficient $\tilde{k}_D^{m/cp}$ of a specific material *m* sliding against a counterpart *cp* is the product of a general material- and roughness-independent dimensional wear coefficient $\tilde{k}_D^*$ and the ratio of the hardnesses H^{cp} and H^m of the contacting surfaces. For the calculation of the wear depth we obtained the differential equation

$$\frac{dh^{m/cp}}{ds} = \underbrace{\tilde{k}_D^* \cdot \frac{H^{cp}}{H^m}}_{\tilde{k}_D^{m/cp}} \cdot \mu(s) \cdot p(s) = \tilde{k}_D^{m/cp} \cdot \mu(s) \cdot \frac{F_N}{A_{real}(s)}, \qquad (1)$$

where $h^{m/cp}$ is the wear depth of the material *m* sliding against a counterpart *cp*, $\mu(s)$ the friction coefficient and $p(s)$ the contact pressure. The wear calculation is then realized with the extended analytical numerical tool named Global Incremental Wear Model (GIWM) [15]. It integrates the unified wear model in dependence of the applied load and sliding velocity based on the present average contact pressure. The average contact pressure is calculated from the global geometry change due to wear and due to the current elastic deformation in contact [14]. In the extended tool [15], important wear influencing contact variables describing the wear- and friction-mechanisms are implemented in form of evolution equations.
They describe, in addition to the development of the linear wear, the surface roughness of the DLC-coating, the oxidation of the steel-counterpart as well as the graphitisation of the DLC-coating based on a single set of material parameters characterising the DLC/steel tribo system. The effect of different coatings is included by easy to access parameters, such as surface roughness, hardness and Young's modulus. The resulting generality of this unified wear model reduces the parameters, which are responsible for the description of wear, to the identification of a single wear coefficient $\tilde{k}_D^*$. The validity of this modelling approach was carefully validated for different types of DLC-coatings and different degrees of surface roughness [15].

Feldfunktion geändert

In this study, the model is used to predict the friction and wear behaviour for different loading histories for the ball-on-plate-geometry and the piston-cylinder-geometry. The predicted wear

behaviour is compared with experimental results with reduced idealisation and different geometry. This represents a further validation of the unified wear model for wear conditions closer to the real application (load variation, component-geometries) and proves its transferability.

2. Experiments

2.1 Experimental setups

To prove the generality of the unified wear model for a modified loading history as well as for a modified geometry we used a standard SRV oscillating sliding wear tester manufactured by Optimol Instruments Prüftechnik GmbH, once with (i) a ball-on-plate geometry, as shown in Figure 1, as well as with (ii) a piston-cylinder-geometry, as shown in Figure 2.

2.1.1 The ball-on-plate-geometry

For the ball-on-plate-geometry, a 100Cr6-steel-ball with a radius $R_b = 2$ mm slides against a flat sample, which can be coated with two different types of DLC-coatings (A and B). The investigated DLC-coatings, differing in elastic modulus and hardness, were deposited on flat 100Cr6-steel samples. The coating's and the 100Cr6 steel's micro-hardness values were measured according to EN ISO 14577-1:2002 and have the following values: A: 24 GPa, B: 42 GPa, and 100Cr6: 14 GPa.

2.1.2 The piston-cylinder-geometry

For the piston-cylinder-geometry, a X90CrMoV18-steel-cylinder with an inside radius of 4.497 ± 0.00135 mm is tested against two different types of DLC-coatings (A and B) on a steel piston with an outside radius of 4.499 ± 0.0005 mm after deposition. The micro-hardness of the cylinder is 14 GPa, the coatings are the same as for the ball-on-plate-geometry.

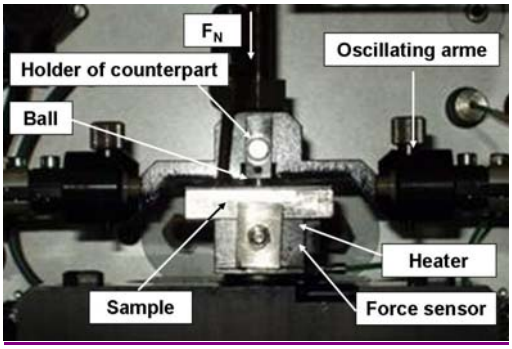

Figure 1: Testing device for oscillating ball-on-plate experiments

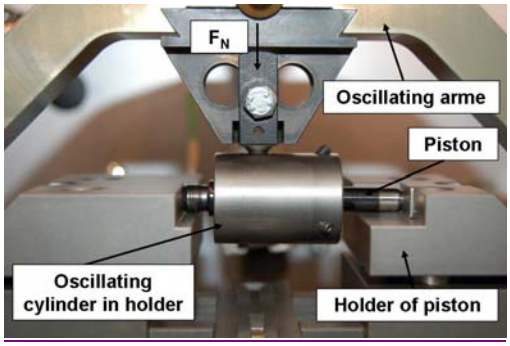

Figure 2: Testing device for oscillating piston-cylinder experiments

2.2. Experimental test parameters

All sliding wear tests are preceded by a running-in phase in order to increase the reproducibility of the measured wear results. The change of the main testing-parameters (force, amplitude and frequency) during the running-in phase and during the subsequent wear test is displayed in Figure 3 respectively 4.

For the ball-on-plate geometry, three different loading conditions are applied after the running-in phase with a mean load of 40 N. Due to its higher wear resistance in comparison to coating A, the load steps for coating B last 10 min longer. The first type of test (1) starts with a sequence of three increasing load steps of 20 N, 40 N and 60 N, where each step lasts 20 min for coating A and 30 min for coating B. The second test (2) applies a constant load of 40 N for 60 min for coating A and 90 min for coating B respectively, and the third test (3) consists of three decreasing load steps of 60 N, 40 N and 20 N, where again each step lasts 20 min for coating A and 30 min for coating B. The frequency and the amplitude are kept constant at 40 Hz and 400 µm, respectively.

The wear of the piston-cylinder-contact is investigated at two different constant loads of 150 N (1) and 300 N (2) for duration of up to 160 h.

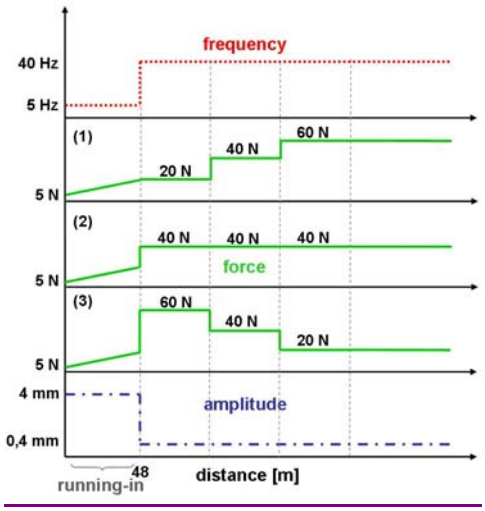

Figure 3: Standard test-parameters for the running-in phase and the subsequent wear test for the ball-on-plate geometry. After 48m of sliding, the parameters are set to the desired test conditions for the wear tests (1) - (3) .

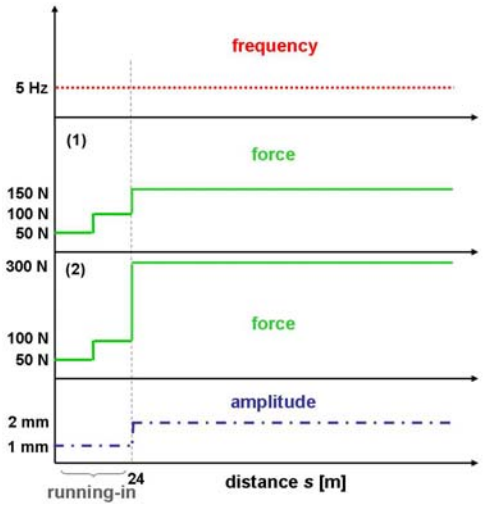

Figure 4: Standard test-parameters for the running-in phase and the subsequent wear test for the piston-cylinder geometry. After 24m of sliding, the parameters are set to the desired test conditions for the wear tests (1) and (2).

For the ball-on-plate-test, it is not possible to interrupt a test in order to measure the wear, so that the wear depth of the coating is measured only at the end of each individual test. The next test has to start with a new pair of samples. In the case of the piston-cylinder-experiment, a continuation after measurement was possible. The wear depth was measured by means of cuts of calottes in the centreline of the wear track.

In this study, we consider only the coating's wear. For the ball-on-plate-geometry, this is due to the fact that the main proportion of the counterpart's wear takes place during the running-in phase [15]. Thus, the effect of the different loading histories on the counterpart's wear is too small and vanishes in the testing scatter. For the piston-cylinder-geometry, the cylinder's wear is not measurable with available measurement technology.

3 Extension of the GIWM

3.1 Loading history for ball-on-plate-geometry

To model different loading histories, the GIWM-routine [15] had to be extended to simulate intervals of different load, different frequency and different endurance as presented in Fig. 3. As the GIWM was already extended from [14] to [15] by adding the running-in phase with linearly increasing load at different frequency, the present modification with adding testing segments at different forces was straight forward and needs no detailed elaboration.

3.2 Transfer to the piston-cylinder-geometry

The original GIWM for ball-on-disc [16] assuming that only the ball wears was extended in earlier works by including the discs wear [14] and for predicting wear in a twin wheel tribometer [17].

In this work, the GIWM is adapted to the piston-cylinder-geometry in order to evaluate the transferability of the unified wear model in accordance to the available validation experiments. The piston-cylinder-geometry is typical for applications of DLC in industry and represents a more realistic situation compared to the ball-on-plate model experiment, which was used to develop the unified wear model and to identify the model parameters.

The initial contact situation in the piston-cylinder-geometry represents a Hertzian line contact, which allows estimating the initial contact area and contact pressure by an analytical solution [18]. The maximum contact pressure $p_{\max}$ along the centreline of the contact can be calculated according to Hertz with

$$p_{\max} = \frac{2 \cdot F_N}{\pi \cdot b \cdot l}. \qquad (2)$$

Here F_N is the normal load, l is the contact length, which corresponds to the length of the cylinder and b is the half width of the contact, given by

$$b = \sqrt{\frac{2 \cdot F_N}{\pi \cdot l} \cdot \frac{2 \cdot R^P \cdot R^C}{R^C - R^P} \cdot \frac{1}{E^*}} \ . \qquad (3)$$

In Eq. (3) R^P is the outside radius of the piston, R^C the inside radius of the cylinder and E^* the reduced elastic modulus. The contact width a, which marks the edge of the wear track A (with $dh^{m/cp}/ds=0$), is approximated by 10-times the half width b of the contact, such that the pressure at A is less than 10 percent of the initial pressure [18] and can be considered as zero.

Formatiert: Schriftartfarbe: Blau

Due to the wear, both the outer surface of the piston and the inner surface of the cylinder will rapidly adapt to each other. This leads to a change in contact geometry, which is represented by R^C and R^P. This conformation is implemented in the GIWM-routine as described in the

following subsections. As the GIWM calculates the wear incrementally in dependence of the sliding cycles i, the equations are formulated appropriately.

The relevant amount of wear relevant is limited to the coating thickness, which is small compared to the dimensions of the piston and cylinder. Thus we can assume that Eqs. (2)-(3) are applicable during the whole lifetime simulation. We calculate the new inner radius R_i^C of the cylinder and the new outside radius R_i^P of the piston with each wear increment, i.e. R_i^C and R_i^P are the radii at the current wear increment *i*. For the calculation loop at step *i* we use R_{i-1}^C and R_{i-1}^P to determine the half width b_i due to Eq. (3) and the contact width $a_i = 10b_i$. The adaptation of R_i^C and R_i^P are described in the following two subsections. Once they are given, we can calculate $(p_{max})_i$ from Eq. (2) and Δh_i from Eq. (1).

Gelöscht: due to

Gelöscht: due to

3.2.1 Adaptation of the inner radius of the cylinder

From the previous wear increment, we assign R_{i-1}^C and R_{i-1}^P. The inside of the cylinder is characterized by a circle of radius R_{i-1}^C with centre point M_{i-1}^C at $(0/0)$. As demonstrated in figure 5 (a) and (b), we select for the following considerations two points P_{i-1} and A_{i-1}, the first in the middle of the contact and the second at the edge of the wear track.

We assume that the cylinder's wear of Δh_i^C is fully effective along the centreline at the contact point $P_{i-1}(0/R_{i-1}^C)$. Thus the old point P_{i-1} is displaced to the new point P_i with the coordinates $P_i : (0/R_{i-1}^C + \Delta h_i^C)$. This implies that the piston will gradually rub itself into the cylinder. The new worn position of the cylinder, respectively of the circle is described with the new cylinder radius R_i^C and the new centre point $M_i^C : (0/(y_i^M)^C)$. In order to recalculate both radius and centre point, we further suppose that the point A_i remains in its position. According to Pythagoras' theorem, its coordinates are determined by the contact width of $2a_i$ and are given by $A_i : (x_i^A / y_i^A) = (a_i / \sqrt{(R_{i-1}^C)^2 - a_i^2})$. As both A_i and P_i lie on the circle determined by R_i^C and M_i^C, we obtain the following.

$$\begin{aligned} ((x_i^A)^C - (x_i^M)^C)^2 + ((y_i^A)^C - (y_i^M)^C)^2 &= (R_i^C)^2 \\ ((x_i^P)^C - (x_i^M)^C)^2 + ((y_i^P)^C - (y_i^M)^C)^2 &= (R_i^C)^2 \end{aligned} \qquad (4)$$

This is an explicit solvable system of equations. With the above constraints, the solutions are

$$(y_i^M)^C = \frac{-2 \cdot R_{i-1}^C \cdot \Delta h_i^C - (\Delta h_i^C)^2}{2 \cdot \sqrt{(R_{i-1}^C)^2 - a_i^2} - 2 \cdot (R_i^C + \Delta h_i^C)}, \quad (5)$$

$$R_i^C = \sqrt{(R_{i-1}^C)^2 - 2 \cdot \sqrt{(R_{i-1}^C)^2 - a_i^2} \cdot (y_i^M)^C + ((y_i^M)^C)^2}. \quad (6)$$

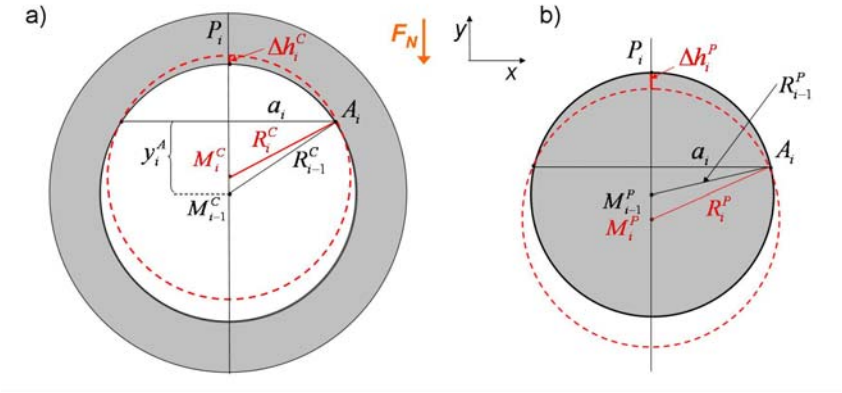

Figure 5: Scheme of the conformation of the piston-cylinder-contact. (a) Adaptation of the inside radius of the cylinder. (b) Adaptation of the outside radius of the piston.

3.2.2 Adaptation of the outer radius of the piston

The adaptation of the outside radius of the piston is realized analogously to the adaptation of the inside radius of the cylinder. Again we describe the outside of the piston by means of a circle with central point M_{i-1}^P at the coordinates $(0/0)$ and a radius R_{i-1}^P. Additionally, we select the points $P_{i-1}: (0/R_{i-1}^P)$ and $A_{i-1}: (x_{i-1}^A / y_{i-1}^A) = (a_i / \sqrt{(R_{i-1}^C)^2 - a_i^2})$ lying on the circle. As shown in figure 5 (b), the point P_{i-1} on the centreline of the contact moves along the negative y-axis with Δh_i^P, the edge point $A_{i-1}=A_i$ remains in its position. Solving the resulting system of equations, we obtain the following expression for the y-coordinate $(y_i^M)^P$ of the new central point $M_i^P: (0/(y_i^M)^P)$ of the outside of the piston in wear increment i,

$$(y_i^M)^P = \frac{2 \cdot R_{i-1}^P \cdot \Delta h_i^P - (\Delta h_i^P)^2}{2 \cdot \sqrt{(R_{i-1}^P)^2 - a_i^2} - 2 \cdot (R_i^P - \Delta h_i^P)}, \quad (7)$$

and the new outside radius of the piston R_i^P,

$$R_i^P = \sqrt{(R_{i-1}^P)^2 - 2 \cdot \sqrt{(R_{i-1}^P)^2 - a_i^2} \cdot (y_i^M)^P + ((y_i^M)^P)^2}. \quad (8)$$

4. Verification of the unified wear model

In this section, the transferability of the unified wear model will be validated by comparing the wear calculations with the experimental results for different loading histories for a ball-on-plate-geometry and for a piston-cylinder-geometry with different but constant load.
As mentioned above, this is realized by comparing the wear calculations - all carried out with the same constant wear coefficient $\tilde{k}_D^*$ - with the experimental results.

4.1 Loading history for ball on plate

Figure 6 and 7 demonstrate the calculated and the experimentally measured wear depths h^c of coating A and B in dependence on the sliding distance s for the above mentioned loading histories. For both coatings we observe a very good agreement between the experimental results and the predicted wear behaviours. The effects of the varying loading history are clearly visible in the experimental data points and the observed phenomena are predicted correctly including the shape of the curves as well as the quantitative effect.

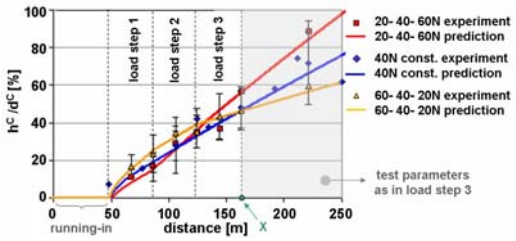

Figure 6: wear depth of the coating A in dependence on the sliding distance for different loading histories.

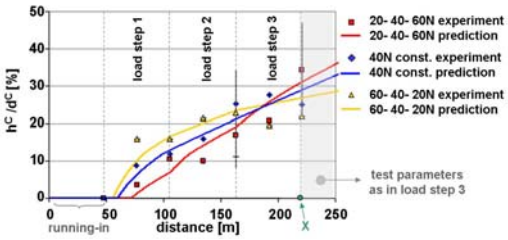

Figure 7: wear depth of the coating B in dependence on the sliding distance for different loading histories.

If we would assume a constant friction coefficient μ and contact area A_{real} in equation (1), we would expect that the wear depends only on the applied normal load and duration. Since all three different loading histories have the same mean normal load, this would lead to an intersection of the wear curves at the end of the third wear step at point X. However, Figure 6 and 7 show that this is not the case. The results clearly support our approach of using evolution equations, which allow integrating the current conditions for friction and wear in form of state variables over the whole loading history.

Interestingly, the results indicate that it is an advantage to induce the high loads in the early part of the loading history.

As the counterpart wears mainly during the first few cycles of the running-in and as the polishing of the surface roughness mainly proceeds during both the running-in and the first load step [15], the predicted real contact pressure p_{real} at the asperities can be assumed to be approximately constant during the second and the third wear step as shown in figure 8 and 9 for the coatings A and B respectively.

Gelöscht: primary

Feldfunktion geändert

Gelöscht: s

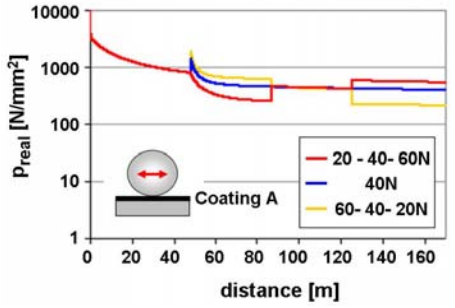

Figure 8: predicted real contact pressure at the asperities of coating A in dependence of sliding distance for different loading histories in ball-on-disc-geometry.

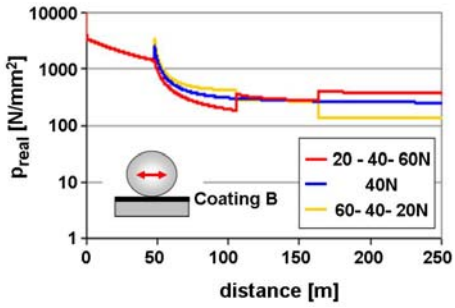

Figure 9: predicted real contact pressure at the asperities of coating B in dependence of sliding distance for different loading histories in ball-on-disc-geometry.

Formatiert: Zentriert

Since the oxide layer is formed within the first cycles, also the ratio of contact hardnesses can also be presumed to be constant. Altogether, this implies that the load- and roughness-dependent friction coefficient is responsible for the advanced intersection of the curves, leading to a lower final wear for the type (3) loading history. The comparison between the predicted and the experimentally measured friction coefficient is presented in Figure 10 for coating A and in Figure 11 for coating B. Both are in good agreement. Only for coating A with type (3) loading history, the experimental measured friction coefficient increases at the end at load step 3 while the predicted behaviour remains at a constant low level. Comparing the curves within Fig. 10 and 11, the initially high load of 60N evidently accelerates the decrease of the friction coefficient in the early stage of the experiment. The higher load increases both the wear of the surface asperities and the contact temperature, leading to an accelerated transformation of the DLC-coating. The agreement with the experimental results verifies the approach of the roughness- and graphitisation-dependent friction coefficient of the unified wear model, as it has been proposed in [15].

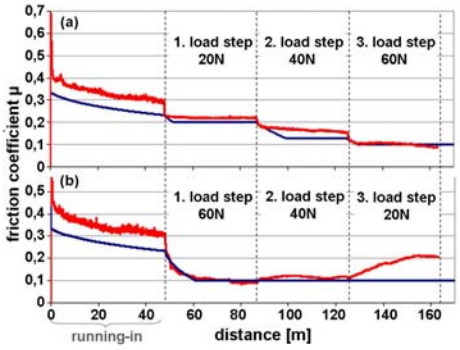

Figure 10: Comparison of predicted and measured friction coefficient μ as a function of sliding distance for coating A and different loading histories. (a) increasing load steps, 20N-40N-60 N, (b) decreasing load steps, 60N-40N-20 N

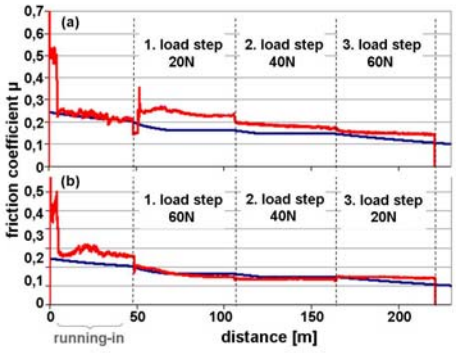

Figure 11: Comparison of predicted and measured friction coefficient μ as a function of sliding distance for coating B and different loading histories. (a) increasing load steps, 20N-40N-60 N, (b) decreasing load steps, 60N-40N-20N

4.2 Piston-cylinder-geometry

In order to prove the transferability of the unified wear model, we use the extended GIWM as described in Sect. 3.2 to apply the wear model to the piston-cylinder geometry. The GIWM's predictions and the experimentally measured wear depths for the coatings A and B (piston) are presented in Figure 12 and 13. For coating A, the wear behaviour has been investigated for 150N and for 300N. For coating B, only data for 300N are given, as the high wear resistance would lead to extremely long test durations at the lower load.

We find a remarkable good agreement between the experimental results and the simulated wear prediction. Only in the case of coating A tested at 150N, the experimental results are below the prediction for very large sliding distances of more than 6000 m. It can not be excluded that inaccuracies during the reassembly after each wear measurement can cause errors in the experiments, which sum up and lead to lower amounts of wear particularly under small load. Despite this uncertainty these results nicely confirm the geometry-independency of the unified wear model and its potential for precise wear and lifetime predictions under conditions as they are present in industrial applications.

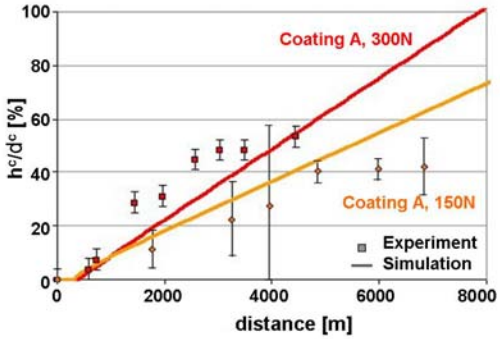

Figure 12: wear depth of coating A in dependence on the sliding distance for 150N and 300N in piston-cylinder-geometry.

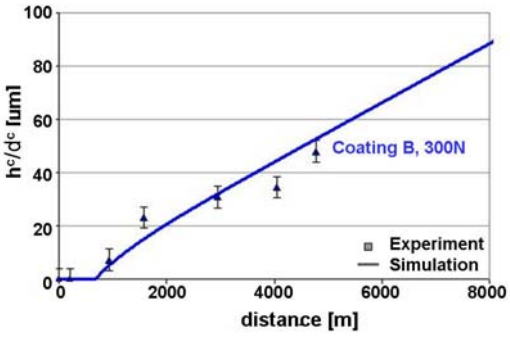

Figure 13: wear depth of coating B in dependence on the sliding distance at 300N in piston-cylinder-geometry.

Gelöscht: 1

Feldfunktion geändert

Figure 14 demonstrates the real contact pressure p_{real} in dependence of the sliding distance s for both coatings A and B in the piston-cylinder-geometry. We can see that after the adaptation of the contacting surfaces and after the polishing of the surface roughness the real contact pressure is stabilized at around 10 N/mm^2. This pressure level is between one and two orders of magnitude smaller compared to the pressure in the accelerated ball-on-plate model experiment (see Figure 8 and 9). The fact that the pressure range used for the model development does not drop near to the level present in the piston-cylinder-geometry underlines the importance of the quantitatively correct predictions presented in Figs. 12 and 13. Hence, the validity of the unified wear model for both geometries is a further demonstration of the generality of the unified wear model.

Gelöscht: at the asperities

Feldfunktion geändert

Gelöscht: In comparison, t

Gelöscht: stabilized

Gelöscht: then

Gelöscht: the real contact

Gelöscht: of

Gelöscht: -geometry

Gelöscht: , which is shown in

Gelöscht: for the coatings A and B respectively

Gelöscht: T

Gelöscht: , although the real contact pressures have different magnitudes,

Formatiert: Schriftart: (Standard) Times New Roman, Nicht Fett

Formatiert: Englisch (Großbritannien)

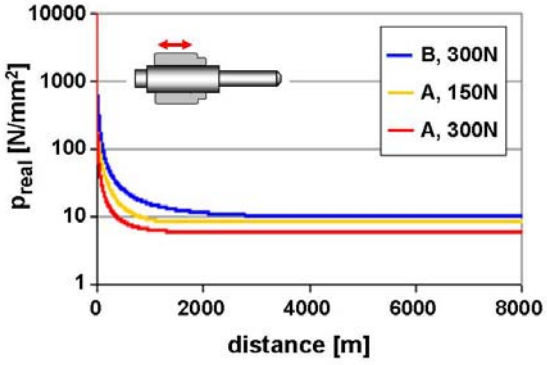

Figure 14: predicted real contact pressure at the asperities of coating A (150N / 300N) and B (300N) in dependence of sliding distance in piston-cylinder-geometry.

5. Conclusions

In this study we successfully validated a novel unified model, which allows predicing the behaviour of friction and wear in DLC/steel contacts for various loading histories and geometrical configurations. In the case of a ball-on-plate-geometry different types of loading histories were applied ranging from steps with increasing, constant, and decreasing load. It was shown that the GIWM implementation of the model accurately predicts both friction and wear behaviour for the different loading histories. Moreover, we could show that higher loads in the initial stages accelerate the generation of graphite, leading to an improved lubrication and lifetime of the component.

The transferability of the wear model to other geometries was shown using a piston-cylinder-geometry with constant load after running-in. The predictions for the different geometry were performed by the extension of the GIWM for the new geometry only and without any adaptation of the wear model or its parameters itself. The agreement between the experimental results and the predictions obtained from the GIWM validates the unified friction and wear model and underlines the importance of considering the whole evolution of the important physical phenomena, such as surface roughness, graphitisation, and oxidation of the counterpart throughout the lifetime of a component.

Formatiert: Schriftartfarbe: Automatisch

Formatiert: Schriftartfarbe: Automatisch

6. Acknowledgement

This work has been financially supported by Robert Bosch GmbH and the German Research Foundation (DFG) under the sub-project T3 within the scope of the collaborative research center, SFB 499 – Design, production and quality assurance of molded microparts constructed from metals and ceramics. We wish to express our thanks to the Robert Bosch GmbH for suggesting the problem and offering us the opportunity to work on it.

7. References

1. C. Donnet, A. Erdemir, Tribology of Diamond-Like Carbon Films, Springer, 2008, p.6.
2. H. Ronkainen, Tribological properties of hydrogenated and hydrogen-free diamond-like carbon coatings, Helsinki University of Technology, Helsinki, Finland 2001, p.38.

3. C. P. O Treutler, Industrial use of plasma-deposited coatings for components of automotive fuel injection systems, Surface and Coating Technology *200* (2005**)** 1969-1975
4. R. Holm, Electric contacts , Almqvist and Wiksells Boktryxkeri AB, Uppsala 1946
5. J. F.Archard, Contact and Rubbing of Flat Surfaces, Journal of Applied Physics 24 (1953) 981-988
6. H. C. Meng, Wear Modeling: Evaluation and Categorization of Wear Models, Phd Thesis, University of Michigan, USA (1994)
7. H. C. Meng, K. C. Ludema, Wear Models and Predictive Equations: Their Form and Content, Wear *181-183* (1995) 443-457
8. J. F. Molinary, M. Ortiz, O. Radovitzzky, E. A. Repetto, Finite Elemente Modeling of Dry Sliding Wear in Metals, Engg. Comput. *18* (2001) 592-609
9. T. F. J. Quinn, Oxidational Wear, Wear *18* (1971) 413-419
10. A. D. Sarkar, Friction and Wear, Academic Press, London (1980)
11. , R. M. Matveesky, The Critical Temperature of Oil with Point and Line Contact Machines, Trans. ASME *87* (1965) 754
12. T. Liskiewicz, S. Fouvry, Development of a friction energy capacity approach to predict the surface coating endurance under complex oscillating sliding conditions, Tribology international 38 (2005) 69-79
13. J. Jiang, R. D. Arnell, On the running-in behaviour of diamond-like carbon coatings under the ball-on-disk contact geometry, Wear 217 (1998) 190-199
14. V. Hegadekatte, N. Huber, O. Kraft, Modeling and simulation of wear in a pin on disc tribometer, Tribology Letters 24 (2006) 51-60.
15. Bitte DGM-Paper einfügen und Referenzen nach hinten updaten!
16. L. Steiner, V. Bouvier, U. May, V. Hegadekatte, N. Huber, Modelling of unlubricated oscillating sliding wear of DLC-coatings considering surface topography, oxidation and graphitisation, submitted for publication, 2009.
17. V. Hegadekatte, N. Huber, O. Kraft: Development of a Simulation Tool for Wear in Microsystems; in Baltes, Brand, Fedder, Hierold, Korvink, Tabata (Eds.): Advanced Micro and Nanosystems, Vol. 4; D. Löhe, J. Hausselt (Volume Eds.): Microengineering of Metals and Ceramics, Part II: Special Replication Techniques, Automation and Properties; Wiley VCH, Weinheim, pp. 605-623, 2005.

Formatiert: Hervorheben

Formatiert: Nummerierung und Aufzählungszeichen

Formatiert: Hervorheben

Formatiert: Nummerierung und Aufzählungszeichen

18. V. Hegadekatte, S. Kurzenhäuser, N. Huber, O. Kraft: A predictive modeling scheme for wear in pin-on-disc and twin-disc tribometers, Tribology International 41 (2008) 1020-1031.

19. J. E. Shigley, C. R. Mischke, Standard Handbook of Machine Design, Kingsport Press. (1986)